

pubs.acs.org/JACS Article

# Ligand-Assisted Direct Lithography of Upconverting and Avalanching Nanoparticles for Nonlinear Photonics

Jia-Ahn Pan, Artiom Skripka, Changhwan Lee, Xiao Qi, Anne L. Pham, Joshua J. Woods, Rebecca J. Abergel, P. James Schuck, Bruce E. Cohen, and Emory M. Chan\*



Cite This: J. Am. Chem. Soc. 2024, 146, 7487–7497



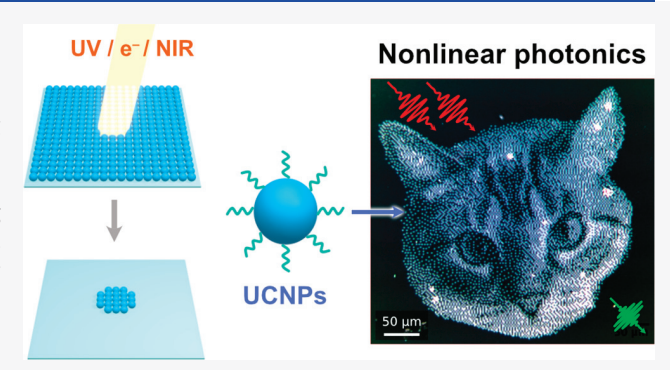
**ACCESS** 

Metrics & More



Supporting Information

ABSTRACT: Upconverting nanoparticles (UCNPs) exhibit unique nonlinear optical properties that can be harnessed in microscopy, sensing, and photonics. However, forming high-resolution nano- and micropatterns of UCNPs with large packing fractions is still challenging. Additionally, there is limited understanding of how nanoparticle patterning chemistries are affected by the particle size. Here, we explore direct patterning chemistries for 6–18 nm Tm<sup>3+</sup>-, Yb<sup>3+</sup>/Tm<sup>3+</sup>-, and Yb<sup>3+</sup>/Er<sup>3+</sup>-based UCNPs using ligands that form either new ionic linkages or covalent bonds between UCNPs under ultraviolet (UV), electronbeam (e-beam), and near-infrared (NIR) exposure. We study the effect of UCNP size on these patterning approaches and find that 6 nm UCNPs can be patterned with compact ionic-based ligands. In



contrast, patterning larger UCNPs requires long-chain, cross-linkable ligands that provide sufficient interparticle spacing to prevent irreversible aggregation upon film casting. Compared to approaches that use a cross-linkable liquid monomer, our patterning method limits the cross-linking reaction to the ligands bound on UCNPs deposited as a thin film. This highly localized photo-/electron-initiated chemistry enables the fabrication of densely packed UCNP patterns with high resolutions ( $\sim$ 1  $\mu$ m with UV and NIR exposure; <100 nm with e-beam). Our upconversion NIR lithography approach demonstrates the potential to use inexpensive continuous-wave lasers for high-resolution 2D and 3D lithography of colloidal materials. The deposited UCNP patterns retain their upconverting, avalanching, and photoswitching behaviors, which can be exploited in patterned optical devices for next-generation UCNP applications.

## 1. INTRODUCTION

Upconverting nanoparticles (UCNPs) are nanoscale light emitters that utilize sequential, 4f–4f transitions in the ladder-like energy levels of lanthanide dopants to combine energy from several low-energy photons into higher-energy emission. These nonlinear processes can be carefully engineered to enable strong upconverted luminescence (UCL), highly nonlinear photon avalanching, and bidirectional photoswitching, making UCNPs useful for applications such as subdiffraction microscopy, optical nanothermometry, nonlinear photonics, and biological imaging. In a biological imaging.

To fully take advantage of their unique properties and integrate them with other components, UCNPs often need to be patterned on surfaces with micro-/nanoscale precision. This capability to fabricate complex, asymmetric arrangements of UCNPs is essential for their use in security tags, <sup>14</sup> upconverting lasers, <sup>15</sup> multicolored displays, <sup>16</sup> non-volatile optical memory, <sup>10</sup> and multiplexed sensor arrays (e.g., for optical, <sup>17,18</sup> temperature, <sup>19</sup> pressure, <sup>20</sup> or chemical sensing). The ability to precisely place UCNPs would augment

fundamental studies on UCNPs, such as exploring interparticle energy transfer mechanisms by thin-film combinatorial experiments or integrating UCNPs in nanophotonic cavities to study their optical behavior in nontrivial environments.

Controlled microscale patterning of UCNP films has been previously realized through inkjet printing, 14,22 photolithography, 23-26 stereolithography, 27-30 or conjugation to 2D protein assemblies, 31 which successfully show the localization of luminescent UCNPs and their potential uses in various applications. Further advances in pattern resolution, uniformity, and UCNP packing fraction will enable the full potential of UNCPs to be efficiently exploited in complex devices.

Received: November 20, 2023 Revised: February 22, 2024 Accepted: February 26, 2024 Published: March 11, 2024



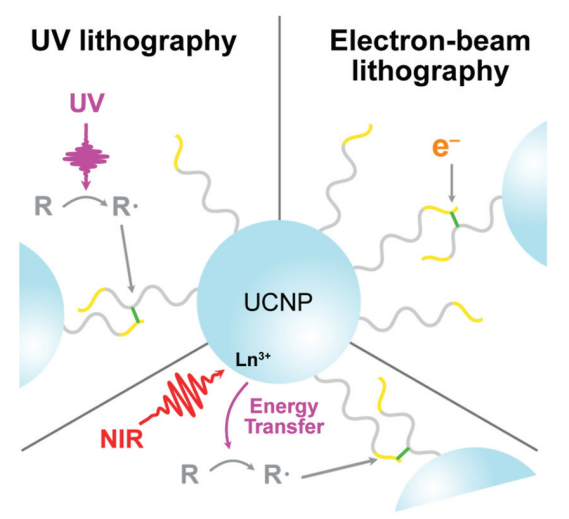


Recently, stimulus-sensitive ligands that respond to light, heat, or electron irradiation have been explored for patterning colloidal nanoparticles (NPs).  $^{32-42}$  This approach circumvents the use of a sacrificial photoresist and allows NPs to be directly patterned with high resolution and uniformity. Two general types of stimulus-sensitive NP ligands have been reported: (1) compact ligands that decompose under UV light, heat, or electron beam exposure and (2) long-chain organic ligands that cross-link under exposure. Although both approaches have been used to fabricate high-resolution patterns of NPs, there needs to be a better understanding of how the NP size affects patterning performance in either case. Because NaYF<sub>4</sub> UCNPs can be synthesized colloidally with diameters ranging from <5 nm nanometers to hundreds of nanometers,  $^{43-45}$  they are a model system to study the effect of size on different patterning chemistries.

Since ligand-based direct lithography approaches have focused on semiconductor (e.g., CdSe and CsPbBr<sub>3</sub>), 35,37,39 and transition metal oxide (e.g., ZrO<sub>2</sub>) NPs,<sup>34</sup> it is an open question whether these approaches are suitable for NPs with fundamentally different chemistries. Besides their broader range in sizes, NaYF4 UCNPs present unique challenges, including their metal fluoride surfaces and their sensitivity to decomposition under aqueous conditions or electron beam irradiation. 46,47 If these challenges were overcome, lanthanidedoped UCNPs could offer a unique nonlinear optical handle that can be exploited for patterning; their ability to upconvert light could allow near-infrared light to be used to activate UVand visible-sensitive compounds that influence UCNP dispersibility and assembly. These direct lithography approaches would be distinct from previous reports using upconverted light for indirect lithography of UCNP/polymer composites, as these reports rely on monomer cross-linking that limits resolution and UCNP packing fraction.<sup>27–30</sup>

Here, we study the patterning chemistries of two different types of stimulus-sensitive ligands through direct ultraviolet (UV), near-infrared (NIR), and electron-beam (e-beam) lithography of lanthanide-doped NaYF<sub>4</sub> UCNPs (Scheme 1). We elucidate chemical design rules for patterning nanoparticles

Scheme 1. Three Types of Stimuli for Patterning UCNPs: UV Light, Near-Infrared Light, and Electron Beam, Shown for UCNPs Coated with Cross-Linkable Ligands



NIR upconversion lithography

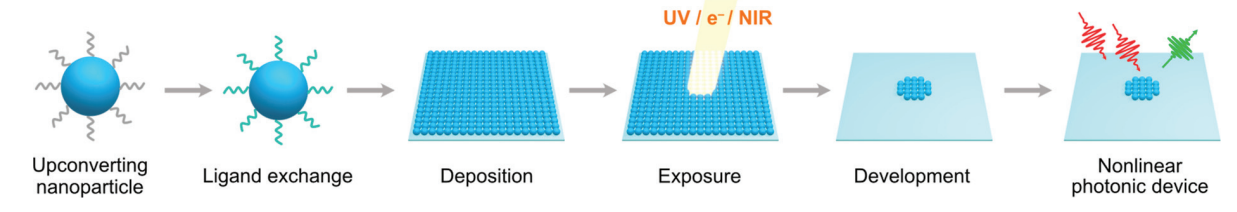
with different diameters by considering how the nanoparticle dispersibility is affected by factors such as ligand photochemistry, interparticle interactions, particle surface preparation, and solvent interactions. Through UV lithography, we find that 6 nm UCNPs can be patterned with a compact photosensitive ionic ligand, but larger 14 nm UCNPs require cross-linkable ligands that keep UCNPs sufficiently spaced apart. The cross-linkable ligands also enable the direct e-beam lithography of UCNPs, with feature sizes <100 nm. We also discover that 980 nm NIR light that is upconverted by Yb<sup>3+</sup>/ Tm<sup>3+</sup>-doped UCNPs can be used in an energy transfer scheme to cross-link these surface ligands, leading to the formation of patterns close to the diffraction-limited beam size. We characterize the optical and chemical properties of the patterned UCNP films and confirm that the UCNPs are densely packed and retain their desirable upconversion luminescence. Finally, we demonstrate proof-of-concept nonlinear optical devices through the patterning of avalanching and photoswitchable UCNPs. Our results establish a general toolbox for direct high-resolution patterning of UCNPs using three different forms of stimuli ranging from high-energy ebeams and traditional UV-light to low-energy NIR light.

## 2. RESULTS AND DISCUSSION

2.1. Direct UV Patterning of UCNPs. 2.1.1. UV Lithography with Photosensitive Ligands That Form New Ionic Linkages. We set out to evaluate whether UCNPs could be printed directly without exogenous photoresists using the method shown in Scheme 2. In this approach, UCNPs coated with photosensitive ligands are spin-cast onto a substrate, irradiated at selected areas, and developed to reveal patterned films of UCNPs. To demonstrate this approach, we started with UV lithography due to its simplicity, high throughput, and widespread availability, making it an optimal choice for parameter screening. We screened a series of nine UV-sensitive ligands ranging from a substituted triazine and azo-benzoic acid to phosphinate and carbamate derivatives. We sought to find ligands that impart high dispersibility for unexposed UCNPs and low dispersibility for exposed UCNPs. However, patterning was not possible for seven of the tested ligands, most commonly because the ligands did not properly functionalize the UCNP surface, resulting in aggregated UCNP films that were permanently nondispersible (see Table S2 for failure modes for each ligand).

We were able to observe successful UCNP patterning with the UV-sensitive ligand, 1-diazo-2-naphthol-4-sulfonic acid (DNS), which we had selected because it was previously used to pattern metal oxide and semiconducting NPs with good fidelities. 34,37 To obtain patterns with DNS, UCNPs were first subjected to an HBF $_4$  ligand stripping approach to remove the native oleate ligand,  $^{48,49}$  transferring UCNPs into a polar DMF solvent (see details in Methods section). The UCNPs were then mixed with DNS with a nominal ligand density of ~2 molecules per nm<sup>2</sup> of UCNP surface (see the Supporting Information for additional discussion), spin-cast as a film on a Si substrate, and irradiated by UV light through a photomask. The UV light is absorbed by DNS (Figure S1A), causing it to transform into 3-sulfo-3H-indene-1-carboxylic acid, which contains a newly formed carboxylic acid group that binds ionically to an adjacent UCNP (Figure 1A). When enough of these binding events have occurred to build up a percolation network, the exposed portion of the UCNP film becomes nondispersible in a DMF developer. Meanwhile, UCNPs that

Scheme 2. Direct Lithography of Upconverting Nanoparticles with Stimulus-Sensitive Ligands



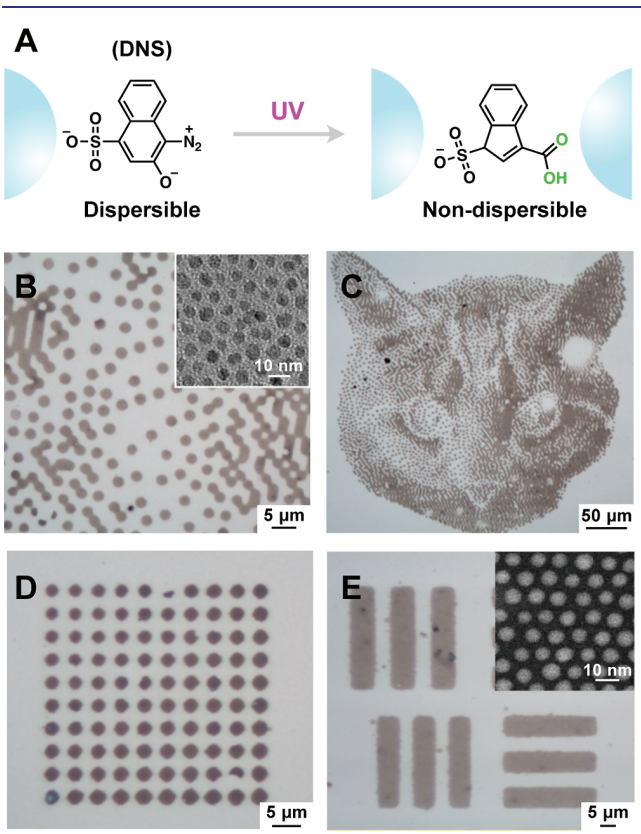


**Figure 1.** UV (395 nm) patterning of UCNPs with diazonaphthosulfonic acid (DNS). (A) DNS is a UV-sensitive ligand that decomposes into a compound with a carboxylate group that links ionically to an adjacent UCNP. (B–E) Optical micrographs of patterns made of 6 nm NaYF<sub>4</sub>: 20% Yb³+, 2% Er³+ UCNPs (B–D) or 6 nm NaYF<sub>4</sub>: 20% Gd³+, 40% Yb³+, 2% Tm³+ UCNPs (E) patterned with DNS using UV light ( $\sim$ 60 mW/cm², 10–30 s). Insets: TEM/STEM images of the UCNPs.

have not been exposed to the UV light are redispersed within the polar DMF solution due to electrostatic repulsion between the charged UCNPs. We have found that the UCNP surface must be only partially covered with DNS ligands, striking a balance between available bare surface access sites and sites already coordinated to DNS ligands. This allows space for DNS, upon photodecomposition, to coordinate with and bridge the partially exposed crystal facets of two adjacent UCNPs. With this process, we obtained microscale patterns of 6 nm cubic-phase NaYF<sub>4</sub>: 20% Yb<sup>3+</sup>, 2% Er<sup>3+</sup> UCNPs (Figure 1B-D). To illustrate that this process is not specific to any dopant composition or crystal phase of NaYF4, we also patterned 6 nm hexagonal phase NaYF<sub>4</sub>: 20% Gd<sup>3+</sup>, 40% Yb<sup>3+</sup>, and 2% Tm<sup>3+</sup> UCNPs (Figure 1E). In contrast, we found that the UCNP size significantly impacts its patternability; we were unable to pattern 14 nm UCNPs despite attempts at

optimizing the ligand-washing steps and DNS fraction. During these attempts, we observed that these larger UCNPs formed nondispersible thin films that resisted development even without exposure to UV light.

2.1.2. Cross-Linkable Ligands Enable UV Lithography with Large UCNPs. The limitations of this DNS patterning approach motivated us to explore alternative stimulus-sensitive ligands that could enable patterning with larger UCNPs. We hypothesized that larger UCNPs have stronger van der Waals (vdW) forces of attraction, which would require bulkier ligands to prevent irreversible NP aggregation that precludes patterning. This led us to the exploration of a second chemical approach that utilizes cross-linkable mono-2-(methacryloyloxy)ethyl succinate (MMES) ligands (Figure 2A), which have been previously used to pattern colloidal quantum dots (QDs). 50 MMES contains a methacrylate endgroup, which is a well-established moiety for free-radical crosslinking that can be initiated by a variety of stimuli (e.g., light, ebeam, and heat), making it a more versatile approach compared to DNS. 51,52 Additionally, compared to oleatecapped UCNPs, MMES-capped UCNPs can be transferred into a polar solvent such as propylene glycol methyl ether acetate (PGMEA), which is a better solvent for many commercial radical initiators.

For this ligand exchange procedure (see details in Methods section), oleate-capped UCNPs were precipitated from their nonpolar solvent and mixed with MMES in PGMEA. A clear, colloidal UCNP solution was obtained after sonication, evidence that most of the nonpolar oleate ligands have been replaced by the polar MMES ligands. For successful patterning, it is important to develop a suitable NP washing procedure to remove desorbed oleic acid and excess MMES, which would prevent UCNPs from aggregating under stimulus exposure. In our initial attempts, we found that the washing method used for QDs (excess ethanol with 5 vol % water) did not work for NaYF<sub>4</sub> UCNPs because the UCNPs were more sensitive to the water content of the solvent. After screening several different solvents, we found hexane to be a suitable nonsolvent for washing the MMES-capped UCNPs dispersed in PGMEA.

With these purified cross-linkable UCNPs, we demonstrated the micropatterning of 14 nm NaYF<sub>4</sub>: 30% Yb<sup>3+</sup>, 0.5% Tm<sup>3+</sup> UCNPs (Figure 2B–E). The cross-linking of MMES ligands was initiated by the UV-sensitive phenylbis(2,4,6-trimethylbenzoyl)phosphine oxide (BAPO) or diphenyl(2,4,6-trimethylbenzoyl) phosphine oxide (TPO) compounds (Figures 2F and S1B). We also investigated the inclusion of the bisphenol A ethoxylate diacrylate (BAED) cross-linker, which was used in a prior report.<sup>50</sup> We found that BAED was not necessary for patterning (Figure S2), but its inclusion resulted in thicker films (due to an increase in the solution viscosity) as well as a longer patterning window (maximum time between deposition and development). Through this process, we obtained high-

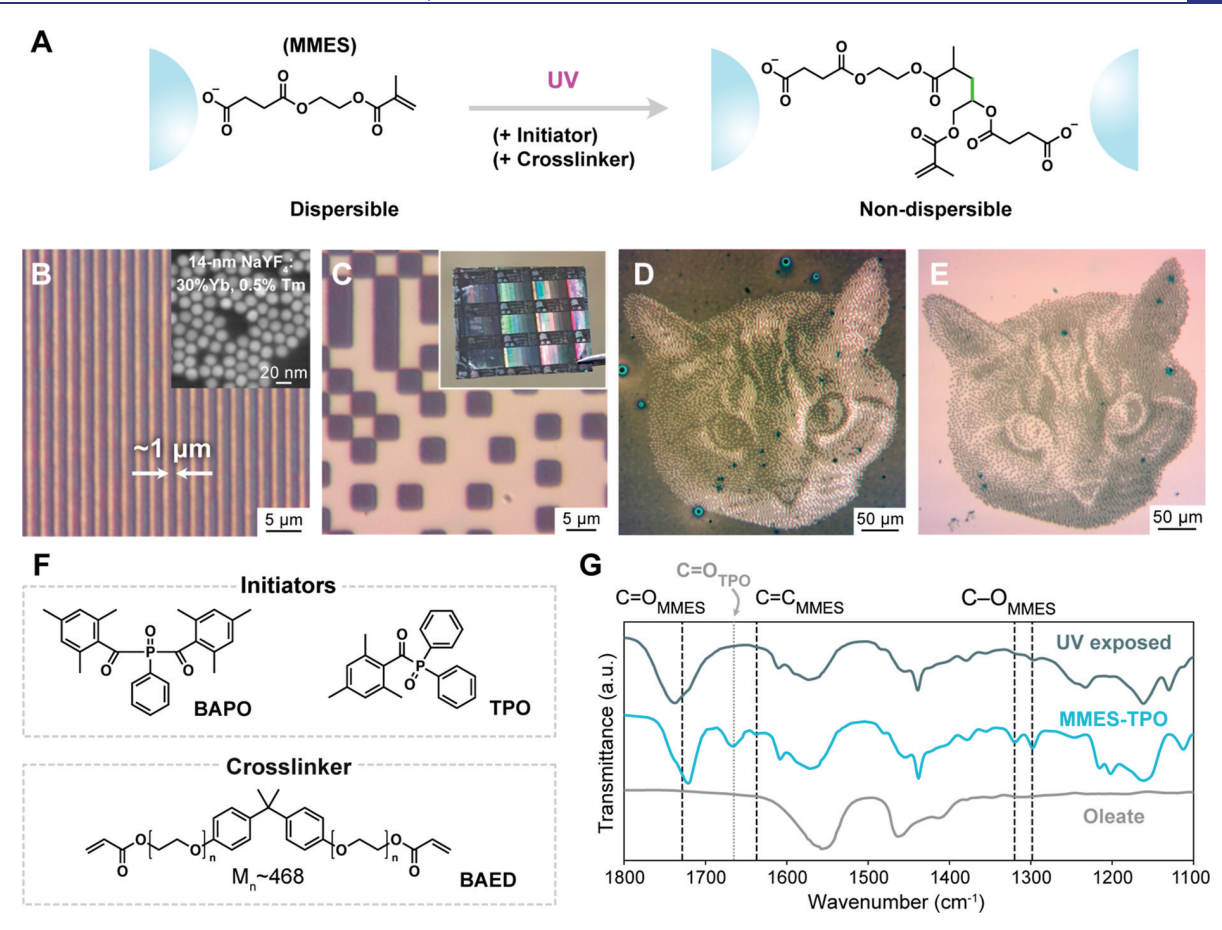


Figure 2. UV (395 nm) patterning of UCNPs by cross-linking ligands. (A) Mono-2-(methacryloyloxy)ethyl succinate (MMES) is a ligand with a double bond that can covalently cross-link with an adjacent MMES ligand upon exposure to a suitable stimulus. (B–E) Optical micrographs of patterns made of MMES-capped 14 nm NaYF<sub>4</sub>: 30% Yb<sup>3+</sup>, 0.5% Tm<sup>3+</sup> UCNPs patterned with UV light ( $\sim$ 60 mW/cm<sup>2</sup>, 10–30 s). Inset for (B): STEM image of the UCNPs. Inset for (C): photograph of a patterned UCNP film on Si. (F) Photoradical initiators and cross-linkers used for MMES-based patterning. (G) FTIR spectra confirming the MMES ligand exchange and cross-linking upon UV exposure.

fidelity micropatterns with feature sizes down to  $\sim$ 1  $\mu$ m, the finest feature on our lithography mask.

Changes in the organic ligand composition during the MMES patterning process were probed by using Fourier transform infrared (FTIR) spectroscopy (Figures 2G and S3). The ligand exchange from oleate into MMES is confirmed through the presence of C=O (1721 cm<sup>-1</sup>), C=C (1637 cm<sup>-1</sup>), and C-O (1320, 1298 cm<sup>-1</sup>) vibrations of MMES (light blue curve), present even after two rounds of washing. We estimate a MMES ligand density of 3.1 molecules/nm<sup>2</sup> through thermogravimetric analysis and NMR (see the Supporting Information for additional discussion). After UV exposure (dark blue curve), the C=O peak (1667 cm<sup>-1</sup>) from TPO disappeared, showing its efficient decomposition. Simultaneously, a significant reduction in the C=C and C-O vibrations of MMES was observed, indicating the formation of new C-C bonds between adjacent MMES ligands consistent with previous reports on methacrylate crosslinking.53,54

2.1.3. Colloidal UCNP Interactions with DNS or MMES Ligands. To explain the differences in our patterning results with DNS and MMES approaches, we considered the underlying microscopic colloidal interactions relevant to the lithography process. Since we experimentally found that irreversible aggregation (nondispersible films) hindered

patternability, we evaluated the fundamental attractive forces that dictate colloidal aggregation.

During the spin-coating process, the evaporation of solvent means that other solvent-based interactions (i.e., electrostatic double-layer and steric interactions) gradually weaken, leaving van der Waals forces as the remaining colloidal interaction. Figure 3A shows the calculated vdW interaction energies for 6 and 14 nm spherical UCNPs as a function of the surface-to-surface distance (the equation and parameters used are shown in eq S1). In the DNS patterning approach, UCNPs approach

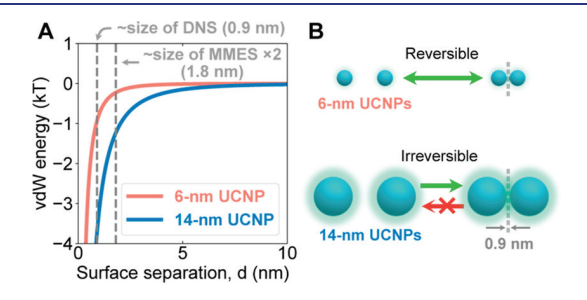


**Figure 3.** (A) Calculated van der Waals (vdW) interaction energy curves for 6 nm NPs and 14 nm UCNPs. (B) Schematic showing that the smaller UCNPs aggregate reversibly, while larger NPs aggregate irreversibly upon drying with a 0.9 nm ligand spacer. The vdW interaction length is indicated by the hazy sphere around the UCNPs.

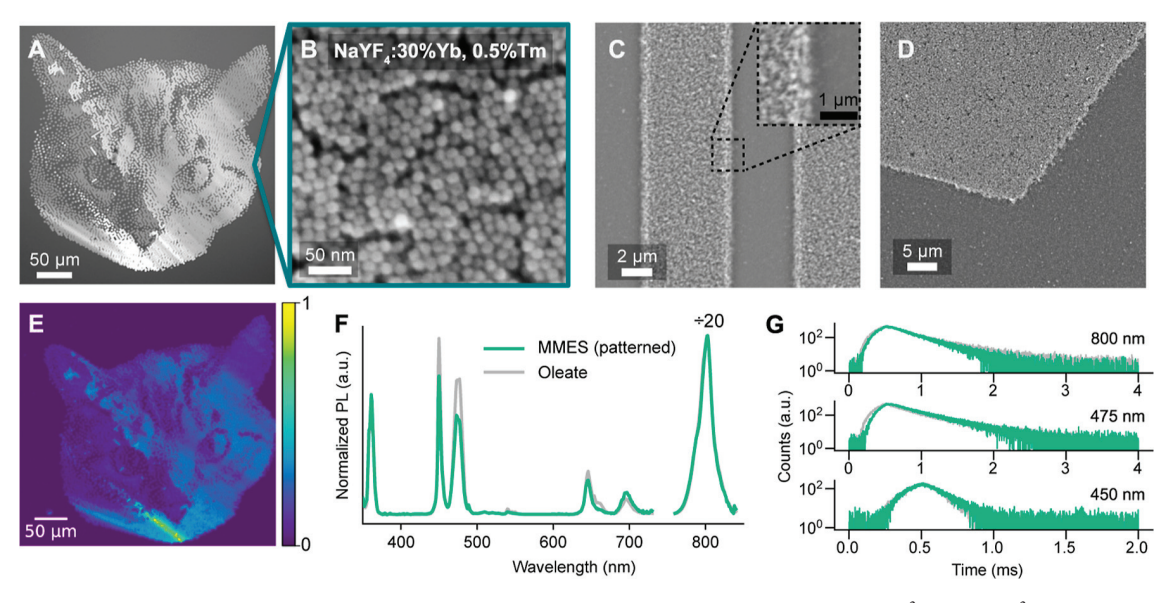


Figure 4. Characterization of UCNP patterns. (A–D) SEM images of 14 nm MMES-capped NaYF<sub>4</sub>: 30% Yb<sup>3+</sup>, 0.5% Tm<sup>3+</sup> UCNPs patterned with UV light. (E) UCL map of the UCNP patterns with 980 nm excitation ( $\sim$ 10<sup>5</sup> W/cm<sup>2</sup>) and visible—NIR emission (400–850 nm). (F,G) Film-level UCL spectra and lifetimes with 980 nm excitation ( $\sim$ 10<sup>2</sup> W/cm<sup>2</sup>) of MMES-patterned UCNPs (with BAPO) and oleate-capped UCNPs. The UCL spectra were normalized to the 800 nm emission peak.

one another until they reach a distance equivalent to the length of the DNS molecule. Only a monolayer of DNS molecules can be added between UCNPs because each DNS molecule needs to be in contact with two adjacent UCNPs for successful photoinduced ionic linking. From the energy curve, we can see that at this distance (~0.9 nm), the vdW interaction energy is smaller for 6 nm UCNPs (~1 kT, Figure 3A—red line) compared to that for 14 nm UCNPs (~4 kT, Figure 3A—blue line). The weaker attraction explains why the smaller 6 nm UCNPs can be easily resuspended in the developer (since the vdW energy is roughly equal to the thermal fluctuations, kT), whereas the larger 14 nm UCNPs tend to aggregate irreversibly (Figure 3B).

For MMES-capped UCNPs, the UCNPs approach each other until they are roughly separated by the length of two MMES ligands (~1.8 nm). From Figure 3A, even the larger 14 nm UNCPs have a reasonably low vdW energy (~1 kT) at these separations, allowing them to be redispersed during development and hence be patternable. Adding BAED cross-linkers can further aid this process by acting as additional physical spacers between UCNPs. We are also exploring the use of compounds such as the hydroxypyridonate-based 3,4,3-LI(1,2-HOPO)<sup>SS</sup> as a spacer for increasing the patterning capabilities of DNS-capped UCNPs, but initial attempts resulted in no improvement in the patternability.

2.1.4. Characterization of UV-Patterned UCNPs. Scanning electron microscopy (SEM) showed the deposition of high-quality patterns of UCNPs (Figure 4A–D). Figure 4A shows an overview SEM image of a microscale patterned feature (this feature has stripes of different thicknesses due to edge effects during spin-coating). UCNPs in the patterned region were densely packed, with surface-to-surface separations on the order of the ligand length (Figure 4B), in stark contrast with prior reports showing relatively sparse packing of UCNPs. SEM reveals no significant qualitative difference in the packing fraction of UCNPs processed with or without BAED (Figure S4) and when compared to the UCNPs before patterning (Figure S5). The edge roughness of the patterns, evaluated

using SEM, is conservatively estimated to be <200 nm (Figure 4C,D).

To determine whether the optical properties of the UCNPs are preserved after the patterning process, we evaluated the UCL properties of the UCNPs on both micro- and macrolevels. First, we carried out UCL mapping of UCNP patterns using a 980 nm laser ( $\sim 10^5$  W/cm²), which confirmed strong UCL from the patterned features (Figure 4E). Additionally, we measured the film-level UCL spectra (Figure 4F) and lifetimes (Figure 4G, fits in Figure S6) of the UCNP patterns and compared them to those of an unpatterned film of oleate-capped UCNPs. We observe no significant difference in both the spectra and lifetimes, showing no appreciable degradation of the optical properties of the UCNPs.

2.2. Electron-Beam Lithography of UCNPs. We investigated the use of e-beam lithography as an approach to achieve submicron features. In principle, e-beam lithography can produce patterns with significantly higher resolution (<10 nm for advanced e-beam writers) than those made through UV lithography. High-precision UCNP patterning via e-beam could facilitate the development of UCNP photonic devices with nanoscale footprint. However, a major challenge in patterning NaYF4 UCNPs with e-beams is the tendency of these UCNPs to degrade upon irradiation by the highly energetic electrons, a common observation when imaging these UCNPs with electron microscopy. 47,56 We thus hypothesized that exchanging the native oleate ligands on these UCNPs with the highly cross-linkable MMES ligands would enable UCNPs to be patterned at low accelerating voltages and doses, reducing the damage to the UCNPs.

When we used imaging SEM to expose MMES-capped UCNPs to e-beam irradiation with relatively modest accelerating voltages (10–15 kV), we observed UCNP patterns with features as small as ~100 nm (Figure 5A–C). Unlike UV lithography, no radical initiator was necessary for e-beam patterning since the high-energy electrons can directly cross-link C=C bonds on the MMES ligands. However, we found that PGMEA could no longer redisperse unexposed

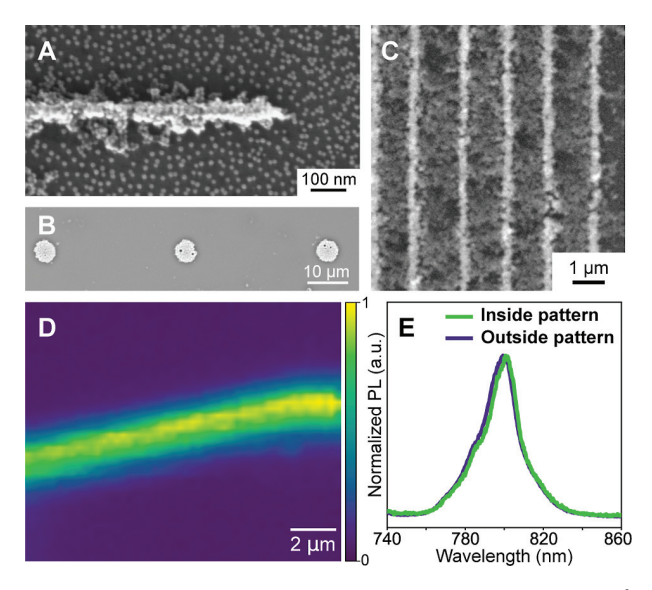


Figure 5. Electron-beam lithography of 14 nm NaYF<sub>4</sub>: 30% Yb<sup>3+</sup>, 0.5% Tm<sup>3+</sup> UNCPs functionalized with MMES ligands. (A) E-beam patterning and imaging with a high-resolution floor model SEM at 10 kV. (B,C) E-beam patterning and imaging with desktop SEM at 15 kV. (D) UCL map of the UCNP patterns with a 980 nm laser ( $\sim 10^5$  W/cm<sup>2</sup>) and 400–850 nm emission. (E) UCL spectra of UCNPs inside the pattern (exposed to the e-beam) and the residual UCNPs outside the pattern (not exposed to the e-beam).

UCNPs after the e-beam patterning process, which we attribute to the aggregation of UCNPs in the SEM vacuum environment. Instead, we found that developing the e-beampatterned films in a 0.1 M HCl solution for a few seconds effectively redispersed unexposed UNCPs, leaving behind deposited patterns of UCNPs. We rationalized that acidic protons can strip the MMES ligands from unexposed UNCPs, rendering them charged and facilitating their dispersion into solution. In contrast, for UCNPs exposed to a sufficient dose of high-energy electrons, the cross-linked MMES ligands act as a barrier that slows access of protons to the UCNP surface, resisting redispersion. We often saw the presence of a sparse residual layer of UCNPs in unexposed regions, which we hypothesize to be due to attractive interactions between the UCNPs and the Si substrate. We believe that this residue can be reduced by optimizing the developer and the washing solvents and passivating the Si surface with self-assembled organic monolayers.

To determine whether UCNPs retain their upconversion properties after exposure to high-energy electrons, we investigated the UCL of e-beam-patterned UCNPs with a 980 nm laser (~10<sup>5</sup> W/cm²). UCL mapping after patterning 14 nm NaYF<sub>4</sub>: 30% Yb³+, 0.5% Tm³+ UNCPs showed strong emission with patterns correlated with those of the deposited features (Figure 5D) and a UCL spectrum comparable to that of residual UCNPs outside the patterning (Figure 5E). These results show that engineering the ligand chemistry of UCNPs opens viable routes for direct e-beam lithography of UCNPs while maintaining their nonlinear optical properties.

**2.3.** Upconversion Near-Infrared Lithography of UCNPs. NIR lithography provides functionalities beyond the more-established UV and e-beam approaches, such as patterning thick layers of material<sup>57</sup> and 3D-printing.<sup>58</sup> An additional advantage of upconversion patterning of UCNPs is that the same optical setup and NIR laser can be used for both

patterning and upconversion microscopy. Compared to two-photon lithography, <sup>59</sup> photon upconversion has been shown to require significantly lower laser powers for 3D stereo-lithography. <sup>60</sup> However, current approaches are lacking in terms of pattern resolution (typically hundreds of micro-meters), <sup>27–30</sup> often due to the use of large (>50 nm) UCNPs that are sparsely dispersed within a liquid of cross-linkable monomers

In principle, high-resolution micropatterning should be achievable through upconversion NIR lithography using densely packed UCNPs coated with cross-linkable ligands. To explore the feasibility of this approach, we scanned specific patterns on a film of MMES-capped, Yb<sup>3+</sup>/Tm<sup>3+</sup>-doped UCNPs with a continuous-wave 980 nm laser. We hypothesized that energy from 980 nm light would be absorbed by Yb<sup>3+</sup> ions, transferred to and upconverted by Tm<sup>3+</sup> ions, and finally transferred radiatively or nonradiatively from higher energy levels of Tm<sup>3+</sup> (e.g., <sup>1</sup>D<sub>2</sub>) to a nearby radical initiator, leading to the cross-linking of MMES ligands on the UCNP surface (Figure 6A).

We tested the upconversion patterning of MMES-capped 14 nm NaYF<sub>4</sub>: 30% Yb<sup>3+</sup>, 0.5% Tm<sup>3+</sup> UCNPs with a range of 980 nm power densities  $(4-34 \times 10^4 \text{ W/cm}^2)$  and dwell times (0.01–10 s). This was done by moving the substrate from spot to spot with an XY piezo stage. Upon the development of the film, we observed deposited patterns of UCNPs that matched our exposure scan patterns (Figure 6B). To confirm that the patterning is not due to the heating of the underlying Si substrate by the laser, we performed a control experiment in which we used the same laser patterning protocol to locally expose 18 nm NaYF<sub>4</sub>: 8% Tm<sup>3+</sup>@NaYF<sub>4</sub> core@shell UCNPs that do not absorb at 980 nm. We did not observe any pattern formation under these conditions (Figure 6C), confirming that the patterns were not formed through a thermal process. This finding is consistent with previous reports that require nanosecond pulsed visible/NIR lasers to achieve sufficient temperatures for thermal patterning of nanomaterials.<sup>33,57</sup>

SEM micrographs (Figure 6D-F) showed the formation of microscale patterns with feature sizes approaching the  $1/e^2$ beam diameter ( $\sim$ 1  $\mu$ m) of our laser at optimal powers and dwell times  $(3.4 \times 10^5 \text{ W/cm}^2, 0.1 \text{ s dwell time})$ . With longer dwell times (a few seconds), we also observed decreased dispersibility in UCNPs as far as  $\sim$ 5  $\mu$ m away from the beam (Figure 6D), which could be caused by Airy rings of the focused laser spot or by long-range radiative energy transfer (in addition to short-range Förster resonance energy transfer found previously<sup>30</sup>). Further lifetime studies with various shell thicknesses should elucidate the details of this energy transfer. We also confirmed that UCNPs patterned by upconversion NIR lithography maintained their UCL properties under 980 nm light (Figure 6G). In summary, our findings reveal that NP-bound MMES ligands enable highly localized cross-linking reactions. These confined photochemical reactions can be initiated by upconverted NIR light, pushing the patterning resolution to  $\sim 1 \mu m$ , a significant improvement over that of state-of-the-art.

**2.4. Patterning Avalanching and Photoswitchable UCNP Microarrays.** To demonstrate the utility of patterned UCNPs, we fabricated proof-of-concept optical memory devices from patterned arrays of avalanching nanoparticles (ANPs). The previously showed that Tm<sup>3+</sup>-doped NaYF<sub>4</sub> ANPs could be repeatedly switched between a luminescent on state to a dark off state using 1064 nm light for

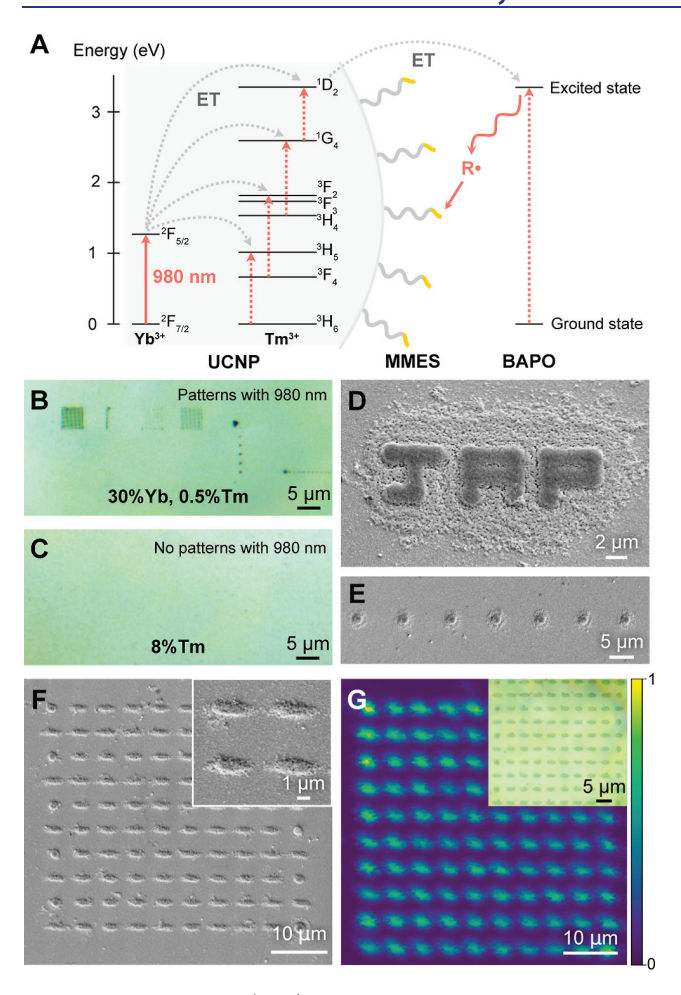


Figure 6. Near-infrared (NIR) upconversion lithography of UCNPs. (A) Simplified scheme for radical-initiated cross-linking of ligands under 980 nm illumination of Yb³+/Tm³+-doped UNCPs mixed with a BAPO radical initiator (ET: energy transfer; R•: radical). (B) Optical micrograph of 14 nm NaYF4: 30% Yb³+, 0.5% Tm³+ UNCPs (mixed with BAPO and BAED) patterned with 980 nm lithography (4–34 × 10⁴ W/cm², 0.01–10 s dwell time). (C) Optical micrographs showing the absence of patterning of 8% Tm³+-doped UCNPs under exposure conditions comparable to those of (B). (D–F) Tilted (30°) SEM images of NIR-patterned UCNPs. (G) UCL map with 980 nm laser excitation (~10⁵ W/cm²) of a patterned array fabricated with the same 980 nm laser (3.4 × 10⁵ W/cm², ~0.1 s dwell time) and 400–850 nm emission. Inset: bright-field microscope image of the patterns.

darkening and 400–840 nm light for brightening. <sup>10</sup> These states are long-lived, enabling high-resolution writing and erasing of persistent 2D and 3D patterns in ANP films. The capability to physically localize these ANP photoswitches would enable more sophisticated interfacing with other optical components (e.g., waveguides and photodetectors), easing their implementation in practical optical memory devices.

We synthesized 9 nm NaYF<sub>4</sub>: 8% Tm<sup>3+</sup> cores, onto which 4.5 nm NaYF<sub>4</sub> shells were grown (18 nm final diameter). After ligand exchange with MMES, these ANPs were mixed with BAPO/BAED and then UV-patterned into arrays of squares with feature sizes of 1  $\mu$ m (Figure 7A,B). The vdW energy between 18 nm UCNPs is calculated to be ca. 2 kT when capped with MMES ligands (Figure S7A). With this interaction energy, the UCNPs can still be patterned without any BAED cross-linker, provided that the spin-coated film is

patterned within 1 min following spin-coating (Figure S7B). However, including BAED cross-linkers prevents the film from drying too fast and allows patterning >1 h after spin-coating. UCL maps of the patterned film under 1064 nm excitation showed localized UCL from patterned features, such as a 2D array of 5  $\mu$ m squares spaced at 10  $\mu$ m periods (Figure 7C). The power dependence of the emission from a patterned feature revealed a nonlinearity factor of  $s \sim 17$  (where  $I_{\rm em} = I_{\rm exc}$ , with s obtained by measuring the 800 nm UCL intensity,  $I_{\rm em}$ , with increasing 1064 nm excitation powers,  $I_{\rm exc}$  and fitting the slope of the log-log plot), consistent with prior reports on unpatterned ANPs (Figure 7D).

To investigate whether patterned ANP arrays can be photoswitched and therefore useful as optical memory devices, we evaluated whether the UCL intensities of specific features can be turned off and on with 1064 and 785 nm NIR lasers. Our initial experiment was a simple photodarkening experiment: we (1) navigated to the desired features under brightfield microscopy, (2) carried out a 1D UCL scan with a 1064 nm laser at low power  $(3 \times 10^4 \text{ W/cm}^2)$ , (3) exposed a selected feature to darken with the 1064 nm laser at high power  $(8 \times 10^5 \text{ W/cm}^2)$ , and (4) repeated steps (2) and (3) for darkening multiple features. With this procedure, we were able to demonstrate the photodarkening of select features that were clearly darker than their surrounding features (Figure 7E). After two photodarkening steps, brightfield imaging showed no visible changes to the features, indicating that the higher laser power internally darkened the ANPs but did not cause morphological damage to the patterns. Finally, we demonstrated bidirectional photoswitching of patterned ANPs with a 1064 nm laser used for UCL measurement (8  $\times$  10<sup>4</sup> W/ cm<sup>2</sup>) and photodarkening (8  $\times$  10<sup>5</sup> W/cm<sup>2</sup>), while a 785 nm laser was used for photobrightening (3  $\times$  10<sup>4</sup> W/cm<sup>2</sup>). With this approach, we demonstrated that a specific 5  $\mu$ m feature can be switched on and off for at least 4 cycles (Figure 7F). No visible signs of pattern degradation were observed even after repeated exposure to the focused NIR laser beam.

## 3. CONCLUSIONS

In summary, we explored two stimulus-sensitive ligand systems that enable the direct lithography of lanthanide-doped NaYF<sub>4</sub> UCNPs through UV, electron-beam, or NIR excitation. Our investigations reveal the importance of considering the NP size when choosing and optimizing a particular ligand patterning approach: direct patterning of larger UCNPs was only achievable when the UCNPs were kept sufficiently spaced apart to prevent irreversible aggregation upon film casting. Using an optimized stimulus-sensitive ligand allowed UCNPs to be patterned with high resolution while retaining their unique upconversion, avalanching, and photoswitchable properties. We revealed that the sensitive and highly localized photochemistry of MMES ligands can be exploited to achieve high-resolution e-beam and upconversion NIR lithography, opening a path toward submicrometer 3D printing with continuous-wave NIR lasers.

These chemical and colloidal insights can be applied to pattern various colloidal nanomaterials for a broad range of applications. Our insights into the impact of nanoparticle size on optimal patterning chemistry and are applicable to the direct lithography of many other colloids and components including proteins, polymers, cells, and 2D materials. Integrating our NIR patternable UCNPs with these systems allows for high-resolution NIR printing of 2D/3D functional

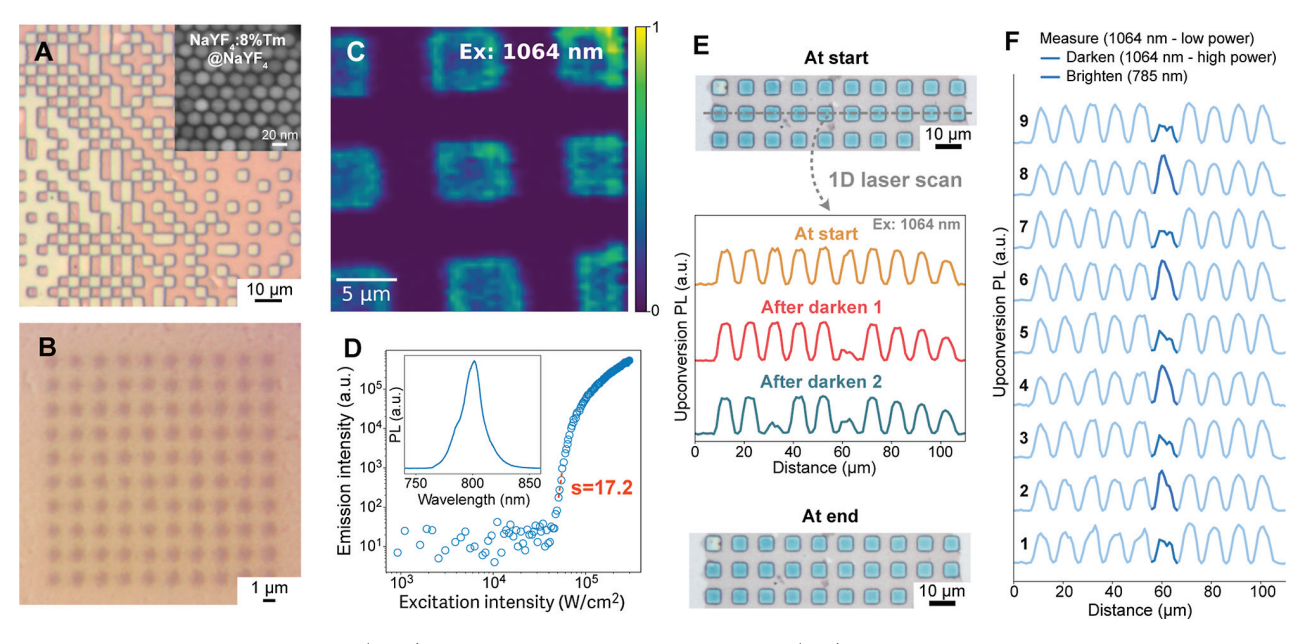


Figure 7. Patterning avalanching UCNP (ANP) arrays with photoswitching capabilities. (A,B) Optical microscopy images of UV-patterned 18 nm ANPs, which were capped with MMES ligands and mixed with BAPO/BAED. (C) UCL of a 5  $\mu$ m patterned array with a 1064 nm laser ( $\sim$ 10<sup>5</sup> W/cm²) and 400–850 nm emission. (D) Power scan of ANPs in a feature showing a highly nonlinear increase in UCL emission with increasing 1064 nm excitation intensity. (E) Sequential photodarkening of two 5  $\mu$ m features with a 1064 nm laser (measurement power: 3  $\times$  10<sup>4</sup> W/cm², darkening power: 8  $\times$  10<sup>5</sup> W/cm²) and detection in the 760–850 nm region. Optical micrographs before and after the photodarkening process show no morphological damage to the features by the laser. (F) Photoswitching demonstration showing that the UCL of a specific feature can be turned on and off repeatedly. Nine sequential measurements were done on the same features, with photodarkening or photobrightening carried out on one feature (highlighted for clarity). Measurement and photodarkening were done with a 1064 nm laser with powers of 8  $\times$  10<sup>4</sup> and 8  $\times$  10<sup>5</sup> W/cm², respectively. Photobrightening was done with a 785 nm laser with a power of 3  $\times$  10<sup>4</sup> W/cm².

structures (e.g., biomaterials and thermoelectric devices) with augmented photophysical properties. The ability to fabricate finely structured patterns of colloidal nanoparticles offers a method to precisely control the interaction of such patterns with chemical and biological constituents. Our patterning approaches utilize widely accessible lithography tools, such as UV projection systems and maskless lasers, allowing them to be scaled up for commercial applications. Additionally, the solution processability of our approach allows UCNPs to be deposited and patterned on virtually any surface (including large and flexible substrates) through scalable deposition methods such as spray-coating and doctor-blading. These advances will accelerate the integration of solution-processed nanomaterials with medical, photonic, and electronic devices (e.g., wearable microsensors, nano-/microprocessors, and bioassays) and enhance their performance within low-cost, compact footprints.

#### 4. METHODS

- **4.1. Reagents.** Mono-2-(methacryloyloxy) ethyl succinate (MMES), bisphenol A ethoxylate diacrylate (BAED, average  $M_{\rm n}$  ~468, EO/phenol 1.5, contains 250 ppm MEHQ as inhibitor), diphenyl(2,4,6-trimethylbenzoyl)phosphine oxide (TPO, 97%), tetrafluoroboric acid diethyl ether complex, and  $N_{\rm s}$ -dimethylformamide (DMF, 99.8%) were purchased from Sigma-Aldrich. Phenylbis(2,4,6-trimethylbenzoyl)phosphine oxide (BAPO, 96.0+%), 1-diazo-2-naphthol-4-sulfonic acid (DNS, 76%), and propylene glycol 1-monomethyl ether 2-acetate (PGMEA, 98.0+%) were purchased from Fisher Scientific.
- **4.2. UCNP Synthesis.** UCNPs were synthesized according to established methods (see the Supporting Information for details).<sup>45</sup>
- **4.3. UCNP Ligand Exchange.** 4.3.1. MMES Ligand Exchange. Ethanol (as a nonsolvent; 1 mL) was added to oleate-capped UCNPs

in hexanes in a 1.5 mL centrifuge tube (100  $\mu$ L, ~10 wt %). The resulting cloudy suspension was centrifuged (5000 rpm, 2012g, 1 min), the supernatant was discarded, and the pellet was redispersed in PGMEA (100  $\mu$ L) to which MMES (~10  $\mu$ L) was added. The cloudy mixture was vortexed and sonicated until a clear dispersion was obtained (typically ~5 min). The UCNPs were then purified with two rounds of hexane/PGMEA washes as follows. First, hexane (400  $\mu$ L) was added to precipitate the UCNPs, and the mixture was centrifuged (5000 rpm, 2012g, 1 min). The pellet was redispersed in PGMEA (100  $\mu$ L) to form a clear dispersion after vortexing. Then, hexane (400  $\mu$ L) was added as a nonsolvent (dispersion remains clear by eye), and the mixture was centrifuged (10,000 rpm, 8049g, 1 min). The clear transparent pellet was finally dissolved in PGMEA at the desired concentration (typically 50 µL for spin-coating, yielding a UCNP concentration of ~10 wt %). The dispersion was sonicated (~20 min) before being used or stored in air. In preparation for UV and NIR lithography, the stock suspension of MMES-capped UCNP solution was first sonicated ( $\sim$ 5 min), and a small amount (10  $\mu$ L) was mixed with a BAPO/TPO photoradical initiator solution (4  $\mu$ L, 30 mg/mL in PGMEA) and a BAED cross-linker solution (2  $\mu$ L, ~50 vol/vol % in PGMEA) right before spin-coating.

4.3.2. DNS Ligand Exchange. Toluene (500  $\mu$ L) was added to oleate-capped UCNPs in hexanes in a 1.5 mL centrifuge tube (100  $\mu$ L, ~10 wt %). Then, 0.5 M HBF<sub>4</sub> in DMF (50  $\mu$ L) was added [the 0.5 M HBF<sub>4</sub> solution was made by slowly adding a tetrafluoroboric acid diethyl ether complex (2.5 mmol, 343  $\mu$ L) to DMF (4.66 mL). Caution: HBF<sub>4</sub> is a strong acid, and this dilution is exothermic]. Adding the HBF<sub>4</sub> solution to the UCNP dispersion leads to the removal of oleate ligands (ligand stripping) and the rapid formation of a precipitate of bare UCNPs (within a few seconds). The suspension is sonicated (~5 min) and centrifuged (5000 rpm, 2012g, 1 min), and the pellet is redispersed in DMF (200  $\mu$ L). The UCNPs were then purified with three rounds of toluene/DMF washes as follows. Toluene (300  $\mu$ L) was added as a nonsolvent to precipitate the UCNPs (the precipitate may not be visible by the eye), and the mixture was centrifuged (5000 rpm, 2012g, 1 min). The transparent

pellet was redispersed in DMF (200  $\mu$ L), toluene (300  $\mu$ L) was added, and the mixture was centrifuged (5000 rpm, 2012g, 1 min). The DMF, toluene, and centrifugation were repeated one more time (three toluene addition steps in total), and the final pellet was dissolved in DMF at the desired concentration (typically ~10 wt % for spin-coating). This suspension can be stored in air for at least a week; long periods lead to gelation of the UCNPs. Before subsequent use, the dispersion was sonicated for ~5 min. Right before spin-coating, a small amount of this bare UCNP dispersion (20  $\mu$ L, ~10 wt %) is mixed with DNS (5  $\mu$ L, 30 mg/mL in DMF).

These ligand exchange procedures can be scaled up with similar results, as long as the volume of the solvents and nonsolvents are scaled proportionally.

**4.4.** Lithography. 4.4.1. UCNP Film Deposition. Silicon substrates (with native oxide) were cut ( $\sim$ 1/2 in.  $\times$  1/2 in.) and cleaned by sonication in acetone ( $\sim$ 5 min) followed by reagent alcohol ( $\sim$ 5 min). The substrates were blown dry with a N<sub>2</sub> gun and subjected to a UV—ozone treatment ( $\geq$ 10 min) right before spin-coating. A typical spin-coating involves pipetting the UCNP dispersion ( $\sim$ 5  $\mu$ L) onto the substrate, followed by a two-stage spinning procedure (e.g., a 1000 rpm spin for 40 s, followed by a 2000 rpm spin for 15 s).

4.4.2. Ultraviolet Lithography. The UCNP-coated substrate was sandwiched between a glass slide and a custom patterned chrome photomask (1 in.  $\times$ 1 in. quartz, 1  $\mu$ m critical dimension, HTA Photomask) and held together with two binder clips. This assembly was then exposed to a 395 nm LED gooseneck lamp (Ulikeled,  $\sim$ 60 mW/cm²) for 10–30 s. The UCNPs were then developed in an appropriate solvent (PGMEA for MMES-capped UCNPs, DMF for DNS-capped UCNPs) for  $\sim$ 10 s and dried with a N<sub>2</sub> gun.

4.4.3. Electron-Beam Lithography. The UCNP-coated substrate was transferred into a table-top (Phenom Pro) or full-size imaging SEM (Zeiss Gemini Ultra-55), operating at 10-15 kV accelerating voltages. UCNPs were selectively exposed to the e-beam by moving the positioning stage in either 2D or 1D imaging mode with dwell times of less than 1 s. The MMES-capped UCNPs were then developed in a 0.1 M HCl solution for  $\sim$ 5 s, rinsed with deionized water, and dried with a  $N_2$  gun.

4.4.4. Upconversion Near-Infrared Lithography. The UCNP-coated substrate was placed under a laser scanning microscope and exposed to a continuous-wave 980 nm NIR laser (power density: 4–31 kW/cm²; dwell times 0.01–10 s). The MMES-capped UCNPs were then developed in PGMEA for  $\sim$ 10 s and dried with a N<sub>2</sub> gun.

#### ASSOCIATED CONTENT

## Supporting Information

The Supporting Information is available free of charge at https://pubs.acs.org/doi/10.1021/jacs.3c12850.

Synthesis and shell growth of UCNPs, characterization techniques, laser scanning microscopy and lithography setup, ligand density estimation, photoswitching setup, unsuccessful photosensitive ligands for patterning UCNPs, absorption spectra of ligands, additional optical microscopy images, additional FTIR spectra, van der Waals equation for two spheres, calculation of the Hamaker constant through Lifshitz theory, additional SEM images, UCL lifetimes and fits, calculated vdW interaction for 18 nm UCNPs, XRD spectra for UCNPs, TEM or STEM images of UCNPs, <sup>1</sup>H NMR of ligands on MMES-capped UCNPs, and thermogravimetric analysis of oleate-capped and MMES-capped UCNPs (PDF)

#### AUTHOR INFORMATION

#### **Corresponding Author**

Emory M. Chan — Molecular Foundry, Lawrence Berkeley National Laboratory, Berkeley, California 94720, United States; ⊚ orcid.org/0000-0002-5655-0146; Email: emchan@lbl.gov

#### **Authors**

Jia-Ahn Pan — Molecular Foundry, Lawrence Berkeley National Laboratory, Berkeley, California 94720, United States; Chemical Sciences Division, Lawrence Berkeley National Laboratory, Berkeley, California 94720, United States; ⊕ orcid.org/0000-0001-6153-8611

Artiom Skripka — Molecular Foundry, Lawrence Berkeley National Laboratory, Berkeley, California 94720, United States; Nanomaterials for Bioimaging Group, Departamento de Física de Materiales, Facultad de Ciencias, Universidad Autónoma de Madrid, Madrid 28049, Spain; orcid.org/ 0000-0003-4060-4290

Changhwan Lee — Department of Mechanical Engineering, Columbia University, New York, New York 10027, United States; Present Address: Department of Materials Science and Engineering, Korea Advanced Institute of Science and Technology (KAIST), Daejeon, 34141 Republic of Korea

Xiao Qi — Molecular Foundry, Lawrence Berkeley National Laboratory, Berkeley, California 94720, United States

Anne L. Pham – Molecular Foundry, Lawrence Berkeley National Laboratory, Berkeley, California 94720, United States

Joshua J. Woods — Chemical Sciences Division, Lawrence Berkeley National Laboratory, Berkeley, California 94720, United States; Department of Nuclear Engineering and Chemistry, University of California, Berkeley, California 94720, United States; orcid.org/0000-0002-6213-4093

Rebecca J. Abergel — Chemical Sciences Division, Lawrence Berkeley National Laboratory, Berkeley, California 94720, United States; Department of Nuclear Engineering and Chemistry, University of California, Berkeley, California 94720, United States; Ocid.org/0000-0002-3906-8761

P. James Schuck — Department of Mechanical Engineering, Columbia University, New York, New York 10027, United States; Occid.org/0000-0001-9244-2671

Bruce E. Cohen — Molecular Foundry, Lawrence Berkeley National Laboratory, Berkeley, California 94720, United States; Division of Molecular Biophysics & Integrated Bioimaging, Lawrence Berkeley National Laboratory, Berkeley, California 94720, United States; orcid.org/ 0000-0003-3655-3638

Complete contact information is available at: https://pubs.acs.org/10.1021/jacs.3c12850

#### Notes

The authors declare no competing financial interest.

#### ACKNOWLEDGMENTS

This work was supported by the U.S. Department of Energy (DOE), Office of Science, Office of Basic Energy Sciences, Chemical Sciences, Geosciences, and Biosciences Division, Separations Program, at the Lawrence Berkeley National Laboratory under Contract no. DE-AC02-05CH11231. Work at the Molecular Foundry was supported by the Office of Science, Office of Basic Energy Sciences, of the U.S.

Department of Energy under Contract no. DE-AC02-05CH11231. A.S. acknowledges support from the European Union's Horizon 2020 research and innovation program under the Marie Skłodowska-Curie Grant Agreement no. 895809 (MONOCLE). C.L. and P.J.S. acknowledge support from the Defense Advanced Research Project Agency (DARPA) Enhanced Night Vision in Eyeglass Form (ENVision) program (no. HR00112220006). P.J.S. also acknowledges support by the National Science Foundation under grant no. CHE-2203510.

## **■ REFERENCES**

- (1) Haase, M.; Schäfer, H. Upconverting Nanoparticles. *Angew. Chem., Int. Ed.* **2011**, 50 (26), 5808–5829.
- (2) Zheng, B.; Fan, J.; Chen, B.; Qin, X.; Wang, J.; Wang, F.; Deng, R.; Liu, X. Rare-Earth Doping in Nanostructured Inorganic Materials. *Chem. Rev.* **2022**, *122* (6), 5519–5603.
- (3) Tian, B.; Fernandez-Bravo, A.; Najafiaghdam, H.; Torquato, N. A.; Altoe, M. V. P.; Teitelboim, A.; Tajon, C. A.; Tian, Y.; Borys, N. J.; Barnard, E. S.; Anwar, M.; Chan, E. M.; Schuck, P. J.; Cohen, B. E. Low irradiance multiphoton imaging with alloyed lanthanide nanocrystals. *Nat. Commun.* **2018**, *9* (1), 3082.
- (4) Homann, C.; Krukewitt, L.; Frenzel, F.; Grauel, B.; Würth, C.; Resch-Genger, U.; Haase, M. NaYF4:Yb,Er/NaYF4 Core/Shell Nanocrystals with High Upconversion Luminescence Quantum Yield. *Angew. Chem., Int. Ed.* **2018**, *57* (28), 8765–8769.
- (5) Zhang, Z.; Skripka, A.; Dahl, J. C.; Dun, C.; Urban, J. J.; Jaque, D.; Schuck, P. J.; Cohen, B. E.; Chan, E. M. Tuning Phonon Energies in Lanthanide-doped Potassium Lead Halide Nanocrystals for Enhanced Nonlinearity and Upconversion. *Angew. Chem., Int. Ed.* **2023**, *62* (1), No. e202212549.
- (6) Skripka, A.; Lee, M.; Qi, X.; Pan, J. A.; Yang, H.; Lee, C.; Schuck, P. J.; Cohen, B. E.; Jaque, D.; Chan, E. M. A Generalized Approach to Photon Avalanche Upconversion in Luminescent Nanocrystals. *Nano Lett.* **2023**, 23 (15), 7100–7106.
- (7) Lee, C.; Xu, E. Z.; Liu, Y.; Teitelboim, A.; Yao, K.; Fernandez-Bravo, A.; Kotulska, A. M.; Nam, S. H.; Suh, Y. D.; Bednarkiewicz, A.; Cohen, B. E.; Chan, E. M.; Schuck, P. J. Giant nonlinear optical responses from photon-avalanching nanoparticles. *Nature* **2021**, 589 (7841), 230–235.
- (8) Bednarkiewicz, A.; Chan, E. M.; Kotulska, A.; Marciniak, L.; Prorok, K. Photon avalanche in lanthanide doped nanoparticles for biomedical applications: super-resolution imaging. *Nanoscale Horiz.* **2019**, *4* (4), 881–889.
- (9) Liang, Y.; Zhu, Z.; Qiao, S.; Guo, X.; Pu, R.; Tang, H.; Liu, H.; Dong, H.; Peng, T.; Sun, L.-D.; Widengren, J.; Zhan, Q. Migrating photon avalanche in different emitters at the nanoscale enables 46th-order optical nonlinearity. *Nat. Nanotechnol.* **2022**, *17* (5), 524–530.
- (10) Lee, C.; Xu, E. Z.; Kwock, K. W. C.; Teitelboim, A.; Liu, Y.; Park, H. S.; Ursprung, B.; Ziffer, M. E.; Karube, Y.; Fardian-Melamed, N.; Pedroso, C. C. S.; Kim, J.; Pritzl, S. D.; Nam, S. H.; Lohmueller, T.; Owen, J. S.; Ercius, P.; Suh, Y. D.; Cohen, B. E.; Chan, E. M.; Schuck, P. J. Indefinite and bidirectional near-infrared nanocrystal photoswitching. *Nature* **2023**, *618*, 951–958.
- (11) Liu, Y.; Lu, Y.; Yang, X.; Zheng, X.; Wen, S.; Wang, F.; Vidal, X.; Zhao, J.; Liu, D.; Zhou, Z.; Ma, C.; Zhou, J.; Piper, J. A.; Xi, P.; Jin, D. Amplified stimulated emission in upconversion nanoparticles for super-resolution nanoscopy. *Nature* **2017**, *543* (7644), 229–233.
- (12) Vetrone, F.; Naccache, R.; Zamarrón, A.; Juarranz de la Fuente, A.; Sanz-Rodríguez, F.; Martinez Maestro, L.; Martín Rodriguez, E.; Jaque, D.; García Solé, J.; Capobianco, J. A. Temperature Sensing Using Fluorescent Nanothermometers. *ACS Nano* **2010**, *4* (6), 3254–3258.
- (13) Pedroso, C. C. S.; Mann, V. R.; Zuberbühler, K.; Bohn, M.-F.; Yu, J.; Altoe, V.; Craik, C. S.; Cohen, B. E. Immunotargeting of Nanocrystals by SpyCatcher Conjugation of Engineered Antibodies. *ACS Nano* **2021**, *15* (11), 18374–18384.

- (14) You, M.; Zhong, J.; Hong, Y.; Duan, Z.; Lin, M.; Xu, F. Inkjet printing of upconversion nanoparticles for anti-counterfeit applications. *Nanoscale* **2015**, *7* (10), 4423–4431.
- (15) Liu, Y.; Teitelboim, A.; Fernandez-Bravo, A.; Yao, K.; Altoe, M. V. P.; Aloni, S.; Zhang, C.; Cohen, B. E.; Schuck, P. J.; Chan, E. M. Controlled Assembly of Upconverting Nanoparticles for Low-Threshold Microlasers and Their Imaging in Scattering Media. *ACS Nano* 2020, 14 (2), 1508–1519.
- (16) Mun, K. R.; Kyhm, J.; Lee, J. Y.; Shin, S.; Zhu, Y.; Kang, G.; Kim, D.; Deng, R.; Jang, H. S. Elemental-Migration-Assisted Full-Color-Tunable Upconversion Nanoparticles for Video-Rate Three-Dimensional Volumetric Displays. *Nano Lett.* **2023**, *23*, 3014–3022.
- (17) Liang, L.; Wang, C.; Chen, J.; Wang, Q. J.; Liu, X. Incoherent broadband mid-infrared detection with lanthanide nanotransducers. *Nat. Photonics* **2022**, *16*, 712–717.
- (18) Lei, L.; Wang, Y.; Kuzmin, A.; Hua, Y.; Zhao, J.; Xu, S.; Prasad, P. N. Next generation lanthanide doped nanoscintillators and photon converters. *eLight* 2022, 2 (1), 17.
- (19) Fischer, L. H.; Harms, G. S.; Wolfbeis, O. S. Upconverting Nanoparticles for Nanoscale Thermometry. *Angew. Chem., Int. Ed.* **2011**, *50* (20), 4546–4551.
- (20) McLellan, C. A.; Siefe, C.; Casar, J. R.; Peng, C. S.; Fischer, S.; Lay, A.; Parakh, A.; Ke, F.; Gu, X. W.; Mao, W.; Chu, S.; Goodman, M. B.; Dionne, J. A. Engineering Bright and Mechanosensitive Alkaline-Earth Rare-Earth Upconverting Nanoparticles. *J. Phys. Chem. Lett.* 2022, *13* (6), 1547–1553.
- (21) Zhang, Z.; Shikha, S.; Liu, J.; Zhang, J.; Mei, Q.; Zhang, Y. Upconversion Nanoprobes: Recent Advances in Sensing Applications. *Anal. Chem.* **2019**, *91* (1), 548–568.
- (22) Lu, Y.; Zhao, J.; Zhang, R.; Liu, Y.; Liu, D.; Goldys, E. M.; Yang, X.; Xi, P.; Sunna, A.; Lu, J.; Shi, Y.; Leif, R. C.; Huo, Y.; Shen, J.; Piper, J. A.; Robinson, J. P.; Jin, D. Tunable lifetime multiplexing using luminescent nanocrystals. *Nat. Photonics* **2014**, *8* (1), 32–36.
- (23) Lee, I.; Park, C.; Kim, T. S.; Kang, M.; Oh, H.; Jang, J.; Park, J.; Yuk, J. M.; Lee, H.; Park, C. B.; Choi, S. Y.; Kang, K.; Lee, W.; Bae, B. S. Water Stable and Photo Patternable Siloxane Encapsulated Upconversion Nanoparticles toward Flexible Near Infrared Phototransistors. *Adv. Opt. Mater.* **2023**, *11* (12), 2202469.
- (24) Kim, W. J.; Nyk, M.; Prasad, P. N. Color-coded multilayer photopatterned microstructures using lanthanide (III) ion co-doped NaYF4 nanoparticles with upconversion luminescence for possible applications in security. *Nanotechnology* **2009**, *20* (18), 185301.
- (25) Kaboli, F.; Ghazyani, N.; Riahi, M.; Zare-Behtash, H.; Majles Ara, M. H.; Heydari, E. Upconverting Nanoengineered Surfaces: Maskless Photolithography for Security Applications. *ACS Appl. Nano Mater.* **2019**, 2 (6), 3590–3596.
- (26) Zhang, X.; Ali, R. F.; Boyer, J.-C.; Branda, N. R.; Gates, B. D. Direct Photolithographic Deposition of Color-Coded Anti-Counterfeit Patterns with Titania Encapsulated Upconverting Nanoparticles. *Adv. Opt. Mater.* **2020**, *8* (20), 2000664.
- (27) Rocheva, V. V.; Koroleva, A. V.; Savelyev, A. G.; Khaydukov, K. V.; Generalova, A. N.; Nechaev, A. V.; Guller, A. E.; Semchishen, V. A.; Chichkov, B. N.; Khaydukov, E. V. High-resolution 3D photopolymerization assisted by upconversion nanoparticles for rapid prototyping applications. *Sci. Rep.* **2018**, 8 (1), 3663.
- (28) Chen, Y.; Zhang, J.; Liu, X.; Wang, S.; Tao, J.; Huang, Y.; Wu, W.; Li, Y.; Zhou, K.; Wei, X.; Chen, S.; Li, X.; Xu, X.; Cardon, L.; Qian, Z.; Gou, M. Noninvasive in vivo 3D bioprinting. *Sci. Adv.* **2020**, 6 (23), No. eaba7406.
- (29) Gao, L.; Zhang, Q.; Gu, M. Photopolymerization induced by up-conversion nanoparticles for three-dimensional low-power nanoscale writing. SPIE/COS Photonics Asia, 2023; Vol. 12322.
- (30) Demina, P. A.; Khaydukov, K. V.; Sochilina, A. V.; Rocheva, V. V.; Ivanov, A. V.; Akasov, R. A.; Lin, Q.; Generalova, A. N.; Khaydukov, E. V. Role of energy transfer in a nanoinitiator complex for upconversion-driven polymerization. *Mater. Today Adv.* **2023**, *19*, 100388.
- (31) Mann, V. R.; Manea, F.; Borys, N. J.; Ajo-Franklin, C. M.; Cohen, B. E. Controlled and Stable Patterning of Diverse Inorganic

- Nanocrystals on Crystalline Two-Dimensional Protein Arrays. *Biochemistry* **2021**, *60* (13), 1063–1074.
- (32) Pan, J. A.; Cho, H.; Coropceanu, I.; Wu, H.; Talapin, D. V. Stimuli-Responsive Surface Ligands for Direct Lithography of Functional Inorganic Nanomaterials. *Acc. Chem. Res.* **2023**, *56* (17), 2286–2297.
- (33) Wu, H.; Wang, Y.; Yu, J.; Pan, J.-A.; Cho, H.; Gupta, A.; Coropceanu, I.; Zhou, C.; Park, J.; Talapin, D. V. Direct Heat-Induced Patterning of Inorganic Nanomaterials. *J. Am. Chem. Soc.* **2022**, *144* (23), 10495–10506.
- (34) Pan, J.-A.; Rong, Z.; Wang, Y.; Cho, H.; Coropceanu, I.; Wu, H.; Talapin, D. V. Direct Optical Lithography of Colloidal Metal Oxide Nanomaterials for Diffractive Optical Elements with  $2\pi$  Phase Control. *J. Am. Chem. Soc.* **2021**, *143* (5), 2372–2383.
- (35) Pan, J.-A.; Ondry, J. C.; Talapin, D. V. Direct Optical Lithography of CsPbX3 Nanocrystals via Photoinduced Ligand Cleavage with Postpatterning Chemical Modification and Electronic Coupling. *Nano Lett.* **2021**, *21* (18), 7609–7616.
- (36) Wang, Y.; Fedin, I.; Zhang, H.; Talapin, D. V. Direct optical lithography of functional inorganic nanomaterials. *Science* **2017**, 357 (6349), 385–388.
- (37) Wang, Y.; Pan, J.-A.; Wu, H.; Talapin, D. V. Direct Wavelength-Selective Optical and Electron-Beam Lithography of Functional Inorganic Nanomaterials. *ACS Nano* **2019**, *13* (12), 13917–13931.
- (38) Pan, J.-A.; Wu, H.; Gomez, A.; Ondry, J. C.; Portner, J.; Cho, W.; Hinkle, A.; Wang, D.; Talapin, D. V. Ligand-Free Direct Optical Lithography of Bare Colloidal Nanocrystals via Photo-Oxidation of Surface Ions with Porosity Control. ACS Nano 2022, 16 (10), 16067–16076.
- (39) Cho, H.; Pan, J. A.; Wu, H.; Lan, X.; Coropceanu, I.; Wang, Y.; Cho, W.; Hill, E. A.; Anderson, J. S.; Talapin, D. V. Direct Optical Patterning of Quantum Dot Light-Emitting Diodes via In Situ Ligand Exchange. *Adv. Mater.* **2020**, 32 (46), 2003805.
- (40) Fu, Z.; Zhou, L.; Yin, Y.; Weng, K.; Li, F.; Lu, S.; Liu, D.; Liu, W.; Wu, L.; Yang, Y.; Li, H.; Duan, L.; Xiao, H.; Zhang, H.; Li, J. Direct Photo-Patterning of Efficient and Stable Quantum Dot Light-Emitting Diodes via Light-Triggered, Carbocation-Enabled Ligand Stripping. *Nano Lett.* **2023**, 23 (5), 2000–2008.
- (41) Liu, D.; Weng, K.; Lu, S.; Li, F.; Abudukeremu, H.; Zhang, L.; Yang, Y.; Hou, J.; Qiu, H.; Fu, Z.; Luo, X.; Duan, L.; Zhang, Y.; Zhang, H.; Li, J. Direct optical patterning of perovskite nanocrystals with ligand cross-linkers. *Sci. Adv.* **2022**, *8* (11), No. eabm8433.
- (42) Hahm, D.; Lim, J.; Kim, H.; Shin, J.-W.; Hwang, S.; Rhee, S.; Chang, J. H.; Yang, J.; Lim, C. H.; Jo, H.; Choi, B.; Cho, N. S.; Park, Y.-S.; Lee, D. C.; Hwang, E.; Chung, S.; Kang, C.-m.; Kang, M. S.; Bae, W. K. Direct patterning of colloidal quantum dots with adaptable dual-ligand surface. *Nat. Nanotechnol.* **2022**, *17*, 952–958.
- (43) Andresen, E.; Islam, F.; Prinz, C.; Gehrmann, P.; Licha, K.; Roik, J.; Recknagel, S.; Resch-Genger, U. Assessing the reproducibility and up-scaling of the synthesis of Er,Yb-doped NaYF4-based upconverting nanoparticles and control of size, morphology, and optical properties. Sci. Rep. 2023, 13 (1), 2288.
- (44) Rinkel, T.; Raj, A. N.; Dühnen, S.; Haase, M. Synthesis of 10 nm  $\beta$ -NaYF4:Yb,Er/NaYF4 Core/Shell Upconversion Nanocrystals with 5 nm Particle Cores. *Angew. Chem., Int. Ed.* **2016**, *55* (3), 1164–1167.
- (45) Ostrowski, A. D.; Chan, E. M.; Gargas, D. J.; Katz, E. M.; Han, G.; Schuck, P. J.; Milliron, D. J.; Cohen, B. E. Controlled Synthesis and Single-Particle Imaging of Bright, Sub-10 nm Lanthanide-Doped Upconverting Nanocrystals. ACS Nano 2012, 6 (3), 2686–2692.
- (46) Torresan, M. F.; Wolosiuk, A. Critical Aspects on the Chemical Stability of NaYF4-Based Upconverting Nanoparticles for Biomedical Applications. *ACS Appl. Bio Mater.* **2021**, *4* (2), 1191–1210.
- (47) Sun, X.; Wang, B.; Kempson, I.; Liu, C.; Hou, Y.; Gao, M. Restructuring and Remodeling of NaREF4 Nanocrystals by Electron Irradiation. *Small* **2014**, *10* (22), 4711–4717.
- (48) Dong, A.; Ye, X.; Chen, J.; Kang, Y.; Gordon, T.; Kikkawa, J. M.; Murray, C. B. A generalized ligand-exchange strategy enabling

- sequential surface functionalization of colloidal nanocrystals. J. Am. Chem. Soc. 2011, 133 (4), 998–1006.
- (49) Nag, A.; Kovalenko, M. V.; Lee, J.-S.; Liu, W.; Spokoyny, B.; Talapin, D. V. Metal-free inorganic ligands for colloidal nanocrystals: S2-HS-Se2-HSe-Te2-HTe-TeS32-OH-and NH2-as surface ligands. *J. Am. Chem. Soc.* **2011**, *133* (27), 10612–10620.
- (50) Hahm, D.; Park, J.; Jeong, I.; Rhee, S.; Lee, T.; Lee, C.; Chung, S.; Bae, W. K.; Lee, S. Surface Engineered Colloidal Quantum Dots for Complete Green Process. ACS Appl. Mater. Interfaces 2020, 12 (9), 10563–10570.
- (51) Huang, J.-Y.; Xu, H.; Peretz, E.; Wu, D.-Y.; Ober, C. K.; Hanrath, T. Three-Dimensional Printing of Hierarchical Porous Architectures. *Chem. Mater.* **2019**, *31* (24), 10017–10022.
- (52) Duan, H.; Winston, D.; Yang, J. K. W.; Cord, B. M.; Manfrinato, V. R.; Berggren, K. K. Sub-10-nm half-pitch electron-beam lithography by using poly(methyl methacrylate) as a negative resist. *J. Vac. Sci. Technol. B* **2010**, 28 (6), C6C58–C6C62.
- (53) Young, A. M. FTIR investigation of polymerisation and polyacid neutralisation kinetics in resin-modified glass-ionomer dental cements. *Biomaterials* **2002**, *23* (15), 3289–3295.
- (54) Delgado, A. H. S.; Young, A. M. Methacrylate peak determination and selection recommendations using ATR-FTIR to investigate polymerisation of dental methacrylate mixtures. *PLoS One* **2021**, *16* (6), No. e0252999.
- (55) Agbo, P.; Müller, A.; Arnedo-Sanchez, L.; Ercius, P.; Minor, A. M.; Abergel, R. J. Amplified luminescence in organo-curium nanocrystal hybrids. *Nanoscale* **2019**, *11* (16), 7609–7612.
- (56) Xu, J.; Tu, D.; Zheng, W.; Shang, X.; Huang, P.; Cheng, Y.; Wang, Y.; Chen, X. Interfacial Defects Dictated In Situ Fabrication of Yolk-Shell Upconversion Nanoparticles by Electron-Beam Irradiation. *Advanced Science* **2018**, *5* (10), 1800766.
- (57) Li, F.; Chen, C.; Lu, S.; Chen, X.; Liu, W.; Weng, K.; Fu, Z.; Liu, D.; Zhang, L.; Abudukeremu, H.; Lin, L.; Wang, Y.; Zhong, M.; Zhang, H.; Li, J. Direct Patterning of Colloidal Nanocrystals via Thermally Activated Ligand Chemistry. *ACS Nano* **2022**, *16* (9), 13674–13683.
- (58) Kawata, S.; Sun, H.-B.; Tanaka, T.; Takada, K. Finer features for functional microdevices. *Nature* **2001**, 412 (6848), 697–698.
- (59) Li, F.; Liu, S.-F.; Liu, W.; Hou, Z.-W.; Jiang, J.; Fu, Z.; Wang, S.; Si, Y.; Lu, S.; Zhou, H.; Liu, D.; Tian, X.; Qiu, H.; Yang, Y.; Li, Z.; Li, X.; Lin, L.; Sun, H.-B.; Zhang, H.; Li, J. 3D printing of inorganic nanomaterials by photochemically bonding colloidal nanocrystals. *Science* **2023**, *381* (6665), 1468–1474.
- (60) Sanders, S. N.; Schloemer, T. H.; Gangishetty, M. K.; Anderson, D.; Seitz, M.; Gallegos, A. O.; Stokes, R. C.; Congreve, D. N. Triplet fusion upconversion nanocapsules for volumetric 3D printing. *Nature* **2022**, 604 (7906), 474–478.